Laboratory Investigations

Targeted Overexpression of Vitamin D Receptor in Osteoblasts Increases Calcium Concentration Without Affecting Structural Properties of Bone Mineral Crystals

B. M. Misof,[1,2] P. Roschger,[1] W. Tesch,[1,2] P. A. Baldock,[3] A. Valenta,[1,2] P. Messmer,[1] J. A. Eisman,[3] A. L. Boskey,[4] E. M. Gardiner,[3] P. Fratzl,[2] K. Klaushofer[1]

[1]Ludwig Boltzmann Institute of Osteology & 4th Med. Dept, Hanusch Hospital & UKH Meidling, Vienna, Austria
[2]Erich Schmid Institute of Materials Science, Austrian Academy of Sciences & University of Leoben, Leoben, Austria
[3]Garvan Institute of Medical Research, Sydney, NSW, Australia
[4]Hospital for Special Surgery, New York, NY 10021, USA

Abstract. Increased cross-sectional area and strength of long bones has been observed in transgenic mice with 2-fold (OSV9) and 3-fold (OSV3) elevation of osteoblast vitamin D receptor (VDR) levels. In the present study, mineralization density distributions, including typical calcium content (Ca_{Peak}) and homogeneity of mineralization (Ca_{Width}) of femoral bone and growth plate cartilage, were determined by quantitative backscattered electron imaging (qBEI). Fourier-transform infrared (FTIR) microspectroscopy was used to examine mineral content, collagen and crystal maturation, and scanning small angle X-ray scattering (scanning-SAXS) for studying mineral particle thickness and alignment. In addition, X-ray diffraction (XRD) of distal tibiae revealed mineral particle c-axis size. In trabecular bone, the increase in Ca_{Peak} was significant for both OSV9 (+3.14%, $P = 0.03$) and OSV3 (+3.43%, $P = 0.02$) versus controls with 23.61 ± 0.45 S.D. wt% Ca baseline values. In cortical bone, Ca_{Peak} was enhanced for the OSV3 mice (+1.84%, $P = 0.02$) versus controls with 26.61 ± 0.28 S.D. wt% Ca, and OSV9 having intermediate values. Additionally, there was significantly increased homogeneity of mineralization as denoted by a reduction of Ca_{Width} (−8.4%, $P = 0.01$) in primary spongiosa. FTIR microspectroscopy, with the exception of an increased collagen maturity in OSV3 trabecular bone (+9.9%, $P = 0.02$), XRD, and scanning-SAXS indicated no alterations in the nanostructure of transgenic bone. These findings indicate that elevation of osteoblastic vitamin D response led to formation of normal bone with higher calcium content. These material properties, together with indications of decreased bone resorption in secondary spongiosa and increased cortical periosteal bone formation, appear to contribute to the improved mechanical properties of their long bones and suggest an important physiological role of the vitamin D-endocrine system in normal bone mineralization.

Key words: Vitamin D receptor — Quantitative Backscattered Electron Imaging (qBEI) — Fourier-Transform Infrared (FTIR) microspectroscopy — Scanning small angle X-ray scattering (scanning-SAXS) — X-ray Diffraction (XRD)

Vitamin D plays an important role in the regulation of calcium homeostasis and bone development, with effects on osteoblastic differentiation and on stimulation of osteoclast recruitment and differentiation [1]. Lack of vitamin D results in rickets in children and osteomalacia in adults. Vitamin D acts predominantly on bone via the nuclear vitamin D receptor (VDR) in osteoblastic cells and osteoclast precursors [2]. The VDR binds 1,25-dihydroxyvitamin D [l, 5-(OH)]$_2$ D], the biologically active form of vitamin D, with high affinity and specificity.

Common allelic variants in the gene encoding the vitamin D receptor have been associated with bone turnover and bone density in some [3–6] but not all [7] populations and the role of the VDR in determination of bone density is still controversial. Recently, mouse models with ablation of the vitamin D receptor have been developed. These mice show a normal skeleton at birth but develop hypocalcemia and hyperparathyroidism shortly after weaning, comparable to hereditary vitamin D-resistant rickets (HVDRR) [8, 9]. While bone volume was not decreased in these mice, the amount of unmineralized bone (osteoid) was increased 15-fold compared to the controls [8]. However, the rachitic bone malformation and growth retardation could be rescued

by dietary calcium supplementation or phosphorus restriction [10]. Interestingly, the targeted overexpression of the VDR in mature osteoblastic cells of OSVDR transgenic mice was associated with an anabolic effect on bone [11], with increased cortical bone formation and decreased trabecular bone resorption. Tibial geometry in these transgene mice was favorably altered, with increased cortical area, moment of inertia and diameter. Mechanical testing of the same bones showed increased stiffness and peak load [11].

The human disorders and murine models with ablation or elevation of the VDR clearly indicate that the VDR plays an important role in bone mineralization. However, the exact mechanisms through which vitamin D and the VDR regulate bone mineralization remain unclear. In order to elucidate any possible relationship between the elevation of osteoblastic VDR and mineralization, we characterized the mineral qualities of bone and cartilage from OSVDR mouse femora [11], using quantitative backscattered electron imaging (qBEI), Fourier transform infrared (FTIR) microspectroscopy, X-ray diffraction (XRD) and scanning small angle X-ray scattering (scanning-SAXS). qBEI shows the mineralization density distribution on the micrometer-scale [12, 13]. The other models provide complementary information on the nanostructure of the bone matrix by measuring relative mineral content and crystal maturation, i.e., crystallinity (FTIR) [14], c-axis particle size (XRD), and mineral particle thickness and alignment (scanning-SAXS) [15]. In the present study, the structure of cortical bone, primary and secondary spongiosa, as well as growth plate of OSVDR distal femora were studied for alterations of mineralization associated with VDR elevation in the OSVDR mouse.

Materials and Methods

Bone Samples

The work described here was performed in compliance with animal care and use guidelines from the Australian National Health & Medical Research Council and the New South Wales state government. Distal femora from three different types of mice were studied: OSV9 and OSV3 mice, two independent OSVDR lines which have 2- and 3-fold elevation in total bone vitamin D receptor (VDR) expression, respectively, and control wild type FVB/N, which is the inbred strain from which the OSVDR lines were derived [11]. Female mice, aged 4 months, had been maintained on normal laboratory chow (1% calcium) from weaning and on a semisynthetic low calcium diet (0.1% Ca) for 4 weeks prior to tissue collection. Femora were collected, fixed and dehydrated; distal halves were embedded in methylmethacrylate and sagittal sections were cut, as previously described [11]. The microstructure of the femora was characterized at different sites: cortical bone at the distal midshaft, trabecular bone (secondary spongiosa), primary spongiosa adjacent to the growth plate and mineralized cartilage in the growth plate. Mineralization density distributions (MDD) were obtained from qBEI analysis of 6 mice from each of the 3 mouse groups. FTIR measurements were performed at cortical bone (distinguishing among endosteal, periosteal and central cortical bone)

and at the primary spongiosa of OSV3, and controls (n = 6 each strain). Scanning-SAXS of cortical (diaphyseal) and epi/metaphyseal bone (not distinguishing between trabecular bone and mineralized cartilage of the meta- and epiphysis) of the distal femur was used for the investigation of the nanostructure of bone from OSV3, OSV9 and control mice (n = 6 each strain). All analyses were performed blinded to the mouse strain.

For the qBEI study, previously sectioned femoral blocks were ground successively by silicon carbide paper of type 800, 1200 and 2400 grid and finally polished with 3 and 1 micron diamond grains on a hard polishing cloth keeping the polishing time as short as possible. The entire procedure was done under water-free conditions to avoid the formation of micro- and ultracracks [16] on a Logitech PM5 instrument (Logitech Ltd., Glasgow, Scottland) using ethylenglycol as lubricant. After carbon coating, the quality of the block surface finish was examined in the SEM by secondary electron imaging for the absence of residual grinding scratches and of surface topography. Further, the appearance of electrical charging effects in shrinking cracks of the embedding material as well as in embedding defects were monitored prior to qBEI measurements. Bone areas close to these artifacts were excluded from qBEI evaluations.

After SEM measurements had been performed for qBEI, either 4 micron sections (for FTIR microspectroscopy) or 200 micron sections (as required for SAXS [15, 17]) were cut from the SEM specimens for further study of the collagen/mineral composite. In addition to these studies of femoral bone samples, XRD data were obtained from distal tibiae of OSV3, OSV9 and control mice.

Quantitative Backscattered Electron Imaging (qBEI)

Mineralization density distribution (MDD) of bone and cartilage from the femora of the three different types of mice was characterized by qBEI (described in detail in previous works [13, 18]). A digital SEM was used with the accelerating voltage of the electron beam adjusted to 20 kV, probe current to 110 pA and a working distance of 15 mm (DSM 962, Zeiss, Oberkochen, Germany). Backscattered electrons were collected by a 4 quadrant semiconductor backscattered electron-detector. Bone and cartilage areas were imaged at 200× nominal magnification, corresponding to a pixel resolution of 1 μm. The calibrated, digital 512 × 512 pixel images were generated by one single frame at a scan speed of 100 s per frame (Fig. 1). Seven images were taken of cortical bone, 3–6 of secondary spongiosa, 6–8 of primary spongiosa and 6–8 of mineralized cartilage per specimen, dependent on sample size and mineralized tissue area per image. The gray-levels of these digital images from the intensity of the signal are proportional to the weight concentration of the mineral in bone, and hence can be used to determine the bone- and cartilage-MDD. Gray-level histograms display percentage of bone area occupied by pixels of each gray-level. The gray-levels are determined by the mean atomic number of the bone material, dominated by the relatively high atomic number of Ca ($Z = 20$) compared to the organic matrix ($Z = 6$) (their final transformation into Ca concentration values is described elsewhere [13, 18]). Hence, qBEI is not sensitive to changes in composition of the organic matrix of bone. Mineralization density was characterized by Ca_{Peak} (synonymous to CaMaxFreq [13, 18]), the most frequently observed calcium content within the specimen (peak position of the histogram), and Ca_{Width}, the peak width of MDD (full width at half maximum, synonymous with FWHM [13, 18]), a measure of the homogeneity of the mineralization (variation of the Ca concentration within the studied tissue). Histogram bin width resolution (resolution of calcium concentration) was 0.17 wt% Ca [13].

Fourier-Transform Infrared (FTIR) Microspectroscopy

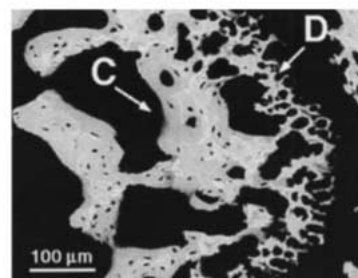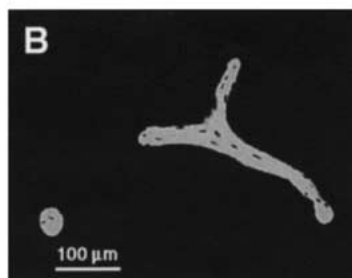FTIR microscopy used a FTS 40 bench microscope interfaced to a UMA 500 microscope (BioRad, Cambridge, MA, USA)
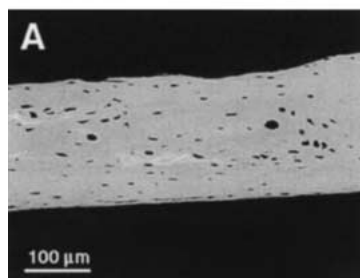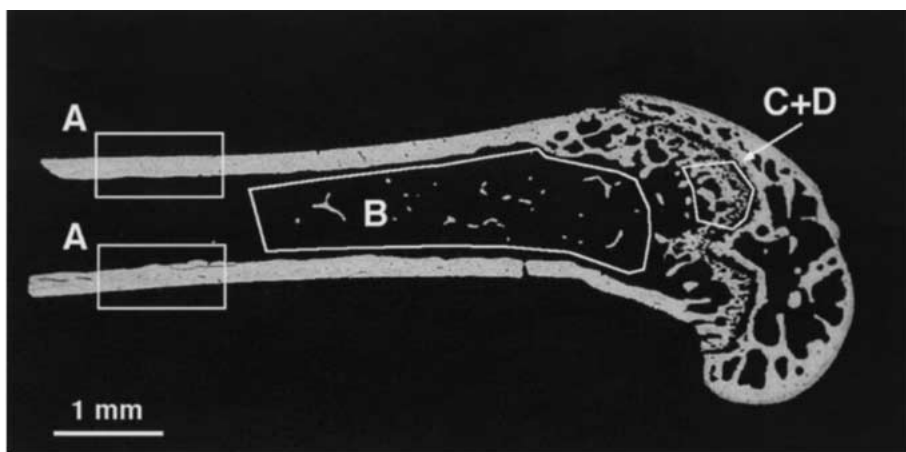
Fig. 1. Areas of the distal femora analyzed by qBEI, FTIR and scanning-SAXS. qBEI was performed separately on cortical bone (**A**), secondary (**B**) and primary (adjacent to growth plate) spongiosa (**C**), and on mineralized cartilage of the growth plate (**D**) (see enlarged images, typical areas). FTIR was carried out at trabecular bone adjacent to the growth plate and at cortical bone (differentiating among endosteal, central, and periosteal areas). Scanning-SAXS was performed on diaphyseal and epi/metaphyseal bone separately, without differentiating between primary spongiosa and growth cartilage at the epiphysis/metaphysis.

with a rotatable mirror to allow sample examination and alignment. Regions of each sample mounted on BaF_2 windows (Spectral Systems, Hopewell Junction, NY) on a computer-controlled X-Y stage (≈ 1 µm precision) were mapped (spatial resolution of 20–100 µm). Spectra were collected from each bone section under nitrogen purge from 3–5 regions of trabecular and from 5–7 regions of cortical bone in each of three distinct 20 µm $\times$ 20 µm areas (adjacent to the periosteum, in the center of the cortex, and adjacent to the endosteum). The interferograms (256 per region) were co-added at 4 cm^{-1} spectral resolution. IR interference from water vapor in the spectrometer and residual embedding agent in the samples was removed by spectral subtraction using a reference spectrum of the embedding agent adjacent to the tissue. Interferograms were apodized with a triangular function, fast Fourier transformed, ratioed against a background spectrum, and converted to absorbance. The relative amount of mineral to organic matter, which is linearly related to the chemically measured ash weight [19], was determined from the ratio of the area of the phosphate ν_1, ν_3 contour to the area of the protein (Amide I). Hence, the mineral to matrix ratio is sensitive to changes in the composition (types of bonds) of both the inorganic and organic phases of the sample. Crystallinity, an index of crystal size and perfection in the c-axis dimension, was estimated from the relative intensities of sub-bands at 1030 and 1020 cm^{-1} [20]. Collagen maturity was estimated based on the relative intensities of sub-bands at 1660 and 1690 cm^{-1} [21].

X-ray Diffraction

Crystallite size and perfection of powdered bone specimens was examined using a Brucker AX-8 powder diffractometer with Ni-filtered CuKα radiation. Proximal tibial halves were ground in a liquid nitrogen cooled freezer mill (SPEX industries, Metuchen, NJ) to ~200 µm size. To provide sufficient bone for analysis, three or four individual ground bones were pooled, providing a total of three pooled samples per group. Using software supplied by the manufacturer, diffraction patterns were K-α stripped, and the line width at half maximum of the 002 peak (β_{002}) was measured. This parameter was then used to calculate the particle size and perfection using the Scherrer equation, with a constant of 0.9.

Scanning SAXS Measurements

Scanning SAXS was performed with a rotating Cu-anode generator (CuKα radiation, wavelength $\lambda = 0.154$ nm, operating at 40 kV/40 mA) and an evacuated pinhole camera (sample to detector distance 1 m) using a two-dimensional, position-sensitive, proportional counter at a spatial resolution of 100 µm (Bruker, AXS, Karlsruhe, Germany) [22]. The sample on a sample holder could be moved automatically with a precision of 2 µm in the plane perpendicular to the beam (beam diameter on the sample = 150 µm). The two-dimensional SAXS patterns of diaphyseal (cortical) and epi/metaphyseal bone of each sample were background corrected and further analyzed for the mean particle thickness parameter T, and the degree of alignment ρ. Considering bone to be a two-phase system consisting of organic and mineral phases with differing electron density [15, 17], particle thickness parameter is defined by $T = 4\,\varphi(1-\varphi)/\sigma$ with φ being the volume fraction of mineral in the tissue and σ the total surface of the mineral crystals per unit volume. T, defined as the total volume fraction per total surface of the particles, is used as a measure of the smallest dimension of needle- or plate-like crystals. From the anisotropy of the scattering patterns, which differ

qualitatively depending on the orientation of the mineral particles within the plane perpendicular to the incident X-ray beam, the degree of alignment ρ can be assessed, reflecting the fraction of non-isotropically aligned particles [22].

Statistical Analysis

Statistical analyses for quantitative backscattered electron imaging data and scanning-SAXS results were calculated using StatView 4.5 (Abacus Concepts, Inc., Berkeley, CA). One-way Anova was followed by Fisher's PLSD test. Values were considered significantly different at $P < 0.05$. Statistical comparisons for FTIR and XRD data were performed using a Bonferroni test for multiple comparisons (GraphPad Instat, GraphPad Software, San Diego, CA) with $P < 0.05$ taken as significant.

Results

Increased Calcium Content and Homogeneity

qBEI analysis (Figs. 2, 3) suggested increases in the typical calcium content (Ca_{Peak}) of all tissues with VDR overexpression compared to control tissues. There was a trend to increased Ca_{Peak} value dependent on the degree of VDR overexpression: Ca_{Peak} was highest in the OSV3 and lowest for the control animals which exhibited baseline values of 23.61 ± 0.45 S.D. wt% Ca (gray level index 161) and 26.61 ± 0.28 S.D. wt% Ca (gray level index 179) for trabecular and cortical bone, respectively. The OSV9 mice revealed intermediate Ca_{Peak} values. This elevation in typical calcium content Ca_{Peak} (+3.14%) was significant for trabecular bone (secondary spongiosa) of OSV9 ($P = 0.03$) and for both trabecular and cortical bone of OSV3 mice, with increases in Ca_{Peak} of +3.43% ($P = 0.02$) and +1.84% ($P = 0.02$), respectively (Fig. 3). Similar but nonsignificant trends were observed in primary spongiosa and epiphyseal cartilage. Homogeneity of mineralization (Ca_{Width}) was not affected by VDR elevation in either trabecular or cortical bone. Unlike the cortical result, however, there was evidence of enhanced homogeneity in primary spongiosa adjacent to the growth plate, denoted by a decrease in Ca_{Width} (−8.42%, $P = 0.01$) for the OSV9 animals. Thus, although by qBEI the average bone calcium content was generally higher in transgenic animals at all bone sites tested, the effect of elevated VDR on homogeneity of mineralization was divergent at the different sites. While mineral content, measured by FTIR and expressed as mineral: matrix ratio, did not differ between the wild type and OSV animals at any site (Table 1), collagen maturity, related to the relative amounts of non-reducible and reducible cross-links [21] was significantly increased in the OSV3 trabecular bone.

Unchanged Mineral Particle Structure

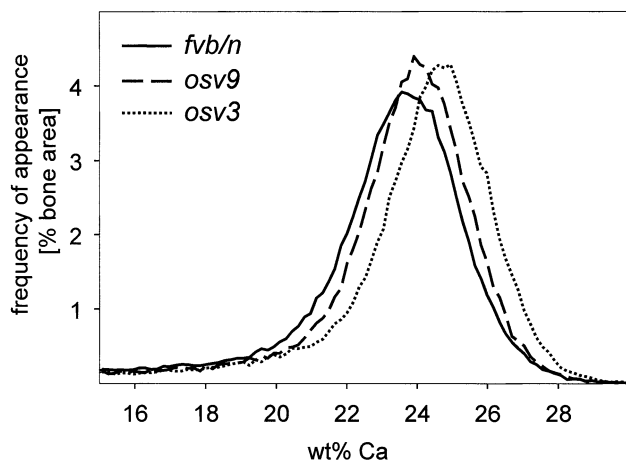Particle size and perfection was not significantly different among the three groups examined (Table 1). Simi-

Fig. 2. Typical MDD of secondary spongiosa as obtained from qBEI. The solid line indicates controls (FVB), the dashed line the OSV9, and the dotted line the OSV3 animals. Note the shift in the peak position of the MDD towards higher mineralization density with increasing degree of VDR elevation.

larly, neither mean mineral particle thickness parameter T nor alignment of mineral particles ρ differed between OSV3 and control mice (Table 1). Independent of genotype, however, T was larger in diaphyseal than in epi/metaphyseal bone, which includes cancellous bone and mineralized cartilage of the growth plate, and mineral particle alignment was less random in diaphysis than in epi/metaphyseal bone (Table 1).

Discussion

The phenotype of OSVDR transgenic mice with elevated VDR in mature osteoblastic cells has been characterized with respect to bone and cartilage mineralization. The combination of four different methods (quantitative backscattered electron imaging, FTIR microspectroscopy, X-ray diffraction, and scanning small angle X-ray scattering) for the investigation of the collagen/mineral composite material has revealed changes associated with VDR overexpression in mature cells of the osteoblastic lineage. This overexpression was associated with a small but significant effect on the mineralization density of bone from the distal femur but without alterations in the nanostructure of the mineralized matrix.

Most interesting, a common finding for all studied regions was the increased typical calcium content in the mineralized matrix of the transgenic animals. Importantly, in no case did the mineral concentration approach pathologically high values, as have been found in the osteogenesis imperfecta mouse model [23, 24]. Increased Ca_{Peak} was observed in both remodeled and non-remodeled tissues such as primary spongiosa and growth plate cartilage, suggesting a role of the VDR in primary mineralization. This is consistent with, but opposite in a sense to, the reduced mineralization evi-
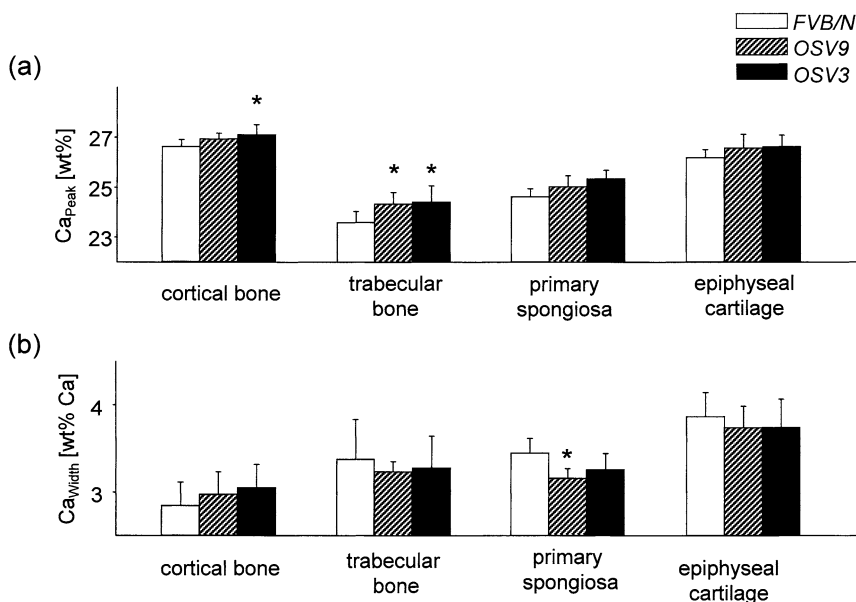
Fig. 3. qBEI results. MDD were characterized by the position (Ca_{Peak}) (a), and the full width at half maximum (Ca_{Width}) of the peak (b). Bar charts correspond to cortical, trabecular bone, primary spongiosa, and mineralized cartilage. White bar = FVB/N controls, striped = OSV9, and black = OSV3. All data shown are mean ± standard deviation. *Indicates statistically significant difference in OSV3 or 9 versus FVB/N ($P < 0.05$, Fishers PLD test).

Table 1. Parameters obtained from FTIR, XRD, and scanning-SAXS

Measured region	Parameter	OSV3	OSV9	FVB/N	P-value
Trabecular bone	Mineral:matrix	5.54 ± 0.34	ND	4.80 ± 0.65	0.16
	Crystallinity	1.07 ± 0.013	ND	1.06 ± 0.02	0.73
	Collagen maturity	3.10 ± 0.06	ND	2.82 ± 0.11	0.015
Center of cortex	Mineral:matrix	6.21 ± 1.3	ND	5.89 ± 0.8	0.73
	Crystallinity	1.06 ± 0.04	ND	1.06 ± 0.02	0.82
	Collagen maturity	2.79 ± 0.28	ND	2.93 ± 0.11	0.49
Cortex adjacent to periosteum	Mineral:matrix	4.54 ± 1.6	ND	4.67 ± 1.6	0.90
	Crystallinity	1.03 ± 0.03	ND	1.07 ± 0.05	0.33
	Collagen maturity	2.73 ± 0.35	ND	3.08 ± 0.03	0.17
Proximal tibia	Crystal c-axis size [nm]	21.7 ± 13.4	25.5 ± 19.6	22.8 ± 12.4	0.90
Diaphyseal bone	T-parameter [nm]	2.36 ± 0.12	2.51 ± 0.17	2.41 ± 0.23	0.35
	ρ	0.36 ± 0.03	0.32 ± 0.09	0.37 ± 0.02	0.24
Epi/metaphyseal bone	T-parameter [nm]	2.13 ± 0.07	2.11 ± 0.05	2.08 ± 0.07	0.38
	ρ	0.25 ± 0.09	0.20 ± 0.09	0.27 ± 0.17	0.54

Values indicate mean ± SD. FTIR and scanning-SAXS parameters were measured in cortical and trabecular bone of the proximal femora, XRD data were obtained from the proximal tibiae. ND = not determined

dent in VDRKO mice, human rickets, and vitamin D-dependent osteomalacia [8, 9, 25–27].

Normal crystallinity (by FTIR) is consistent with the formation of structurally normal bone. XRD- and scanning-SAXS parameters of transgenic femora are also consistent with this interpretation. The 1030/1020 ratio, indicative of crystallite size and perfection (maturity), was not changed, nor was mineral particle thickness parameter T or the degree of mineral particle alignment ρ. The normal nanostructure of OSVDR bone contrasts with structural changes noted in other mouse models [24, 28–30].

In previous investigations of the OSVDR phenotype, the transgene-associated elevation of cortical bone area and strength was independent of dietary calcium, whereas the reduction in trabecular resorption was evident only in mice fed reduced Ca [33]. In the present study, dietary Ca was reduced to allow examination of the material properties of transgenic bones under conditions in which OSVDR cortical bone formation and trabecular resorption phenotypes are both evident. The increase in cortical Ca concentration detected by qBEI in the present study is consistent with the increased strength of transgenic bone [11] and the established relationships among mineralization, stiffness, and strength [31, 32]. In addition, the increased homogeneity of trabecular bone mineralization and collagen maturity in OSVDR primary spongiosa is consistent with an increased trabecular bone tissue age as a result of decreased bone turnover in the transgenic mice [11]. The

present data on the phenotype of these OSVDR mice thus support a role of the vitamin D pathway in primary mineralization as a key regulator of normal mineralization and consequently material quality of bone, independent of calcium homeostasis. The improved mechanical quality of bone associated with VDR elevation indicates an important role for the vitamin D pathway in bone strength and suggests possible therapeutic targets.

References

1. Kraichely DM, MacDonald PN (1998) Transcriptional activation through the vitamin D receptor in osteoblasts. Front Biosci 3:d821–833

2. Kato S (2000) The function of vitamin D receptor in vitamin D action. J Biochem 127:717–722

3. Morrison NA, Yeoman R, Kelly PJ, Eisman JA (1992) Contribution of trans-acting factor alleles to normal physiological variability: vitamin D receptor gene polymorphisms and circulating osteocalcin. Proc Natl Acad Sci 89:6665–6669

4. Morrison N7A, Qui JC, Tokita A, Kelly PJ, Crofts L, Nguyen TV, Sambrook PN, Eisman JA (1994) Prediction of bone density from vitamin D receptor alleles. Nature 367:284–287

5. Spector TD, Keen RW, Arden NK et al. (1995) Influence of vitamin D receptor genotype on bone mineral density in postmenopausal women: a twin study in Britain. BMJ 310:1357–1360

6. Uitterlinden AG, Weel AE, Burger H, Fang Y, van Duijn A, Hofman A, van Leeuwen JP, Pols HA (2001) Interaction between the vitamin D receptor gene and collagen type I alpha 1 gene in susceptibility for fracture. J Bone Miner Res 16:379–385

7. Valimaki S, Tahtela R, Kainulainen K, Laitinen K, Loyttyniemi E, Sulkava R, Valimaki M, Kontula K (2001) Relation of collagen type I alpha 1 (COLIA 1) and vitamin D receptor genotypes to bone mass, turnover, and fractures in early postmenopausal women and to hip fractures in elderly people. Eur J Intern Med 12:48–56

8. Li YC, Pirro AE, Amling M, Delling G, Baron R, Bronson MB, Demay MB (1997) Targeted ablation of the vitamin D receptor: an animal model of vitamin D-dependent rickets type II with alopecia. Proc Natl Acad Sci 94:9831–9835

9. Yoshizawa T, Handa Y, Uematsu Y, Takeda S, Sekine K, Yoshihara Y, Kawakami T, Arioka K, Sato H, Uchiyama S, Masushige S, Fukamizu A, Matsumoto T, Kato S (1997) Mice lacking the vitamin D receptor exhibit impaired bone formation, uterine hypoplasia and growth retardation after weaning. Nature Genet 16:391–396

10. Masuyama R, Nakaya Y, Tanaka S, Tsurukami H, Nakamura T, Watanabe S, Yoshizawa T, Kato S, Suzuki K (2001) Dietary phosphorus restriction reverses the impaired bone mineralization in vitamin D receptor knockout mice. Endocrinology 142:494–497

11. Gardiner EM, Baldock PA, Thomas GP, Sims NA, Henderson KN, Hollis B, White CP, Sunn KL, Morrison WR, Walsh WR, Eisman JA (2000) Increased formation and decreased resorption of bone in mice with elevated vitamin D receptor in mature cells of the osteoblastic lineage. FASEB J 14:1908–1916

12. Boyde A, Maconnachie E, Reid SA, Delling G, Mundy GR (1986) SEM in bone pathology: review of methods, potential and applications. Scanning Electron Microsc IV:1537–1554

13. Roschger P, Fratzl P, Eschberger J, Klaushofer K (1998) Validation of quantitative backscattered electron imaging for the measurement of mineral density distribution in human bone biopsies. Bone 23:319–326

14. Camacho NP, Rinnerthaler S, Paschalis EP, Mendelsohn AL, Boskey AL, Fratzl P (1999) Complementary information on bone ultrastructure from scanning small angle X-ray scattering and Fourier-transform infrared microspectroscopy. Bone 25:287–293

15. Fratzl P, Schreiber S, Klaushofer K (1996) Bone and mineralization as studied by small-angle X-ray scattering. Connect Tissue Res 34:247–254

16. Roschger P, Eschberger J, Plenk H Jr (1993) Formation of ultracracks in methacrylate-embedded undecalcified bone samples by exposure to aqueous solutions. Cells Mater 3:361–365

17. Fratzl P, Groschner M, Vogl G, Plenk Jr. H, Eschberger J, Fratzl-Zelman N, Koller K, Klaushofer K (1992) Mineral crystals in calcified tissues: a comparative study by SAXS. J Bone Miner Res 7:329–334

18. Roschger P, Plenk Jr H, Klaushofer K, Eschberger J (1995) A new scanning electron microscopy approach to the quantification of bone mineral density distribution: backscattered electron image grey-levels correlated to calcium Kα-line intensities. Scan Microsc 9:75–88

19. Pienkowski D, Doers TM, Monier-Faugere MC, Geng Z, Camacho NP, Boskey AL, Malluche HH (1997) Calcitonin alters bone quality in beagle dogs. J Bone Miner Res 12:1936–1943

20. Paschalis EP, Betts F, DiCarlo E, Mendelsohn R, Boskey AL (1997) FTIR microspectroscopic analysis of normal human cortical and trabecular bone. Calcif Tissue Int 61:480–486

21. Paschalis EP, Verdelis K, Doty SB, Boskey AL, Mendelsohn R, Yamauchi M (2001) Spectroscopic characterization of collagen cross-links in bone. J Bone Miner Res 16:1821–1828

22. Rinnerthaler S, Roschger P, Jakob HF, Nader A, Klaushofer K, Fratzl P (1999) Scanning small angle X-ray scattering analysis of human bone sections. Calcif Tissue Int 64:422–429

23. Camacho NP, Landis WJ, Boskey AL (1996) Mineral changes in a mouse model of osteogenesis imperfecta detected by Fourier transform infrared microscopy. Connect Tissue Res 35:259–265

24. Grabner B, Landis WJ, Roschger P, Rinnerthaler S, Peterlik H, Klaushofer K, Fratzl P (2001) Age- and genotype-dependence of bone material properties in the osteogenesis imperfecta murine model (oim). Bone 29:453–457

25. Hughes MR, Malloy PJ, Kieback DG, Kesterson RA, Pike JW, Feldman D, O'Malley BW (1988) Point mutations in the human vitamin D receptor gene associated with hypocalcemia rickets. Science 242:1702–1705

26. Stone T, Max SJ, Lieberman UA, Pike JW (1990) A unique point mutation in the human vitamin D receptor chromosomal gene confers hereditary resistance to the 1,25-dihydroxyvitamin D3. Mol Cell Endocrinol 4:623–631

27. Bikle DD (1999) Drug-induced osteomalacia (Chapter 68), primer on the metabolic bone diseases and disorders of mineral metabolism, 4th ed. Lippincott Williams and Wilkins, Philadephia PA

28. Boskey AL, Gadaleta S, Gundberg C, Doty SB, Ducy P, Karsenty G (1998) FTIR microspectroscopic analysis of bones of osteocalcin-deficient mice provides insight into the function of osteocalcin. Bone 23:187–196

29. Xu T, Fisher L, Bianco P et al. (1998) Targeted disruption of the biglycan gene leads to osteoporosis in mice. Nature Genet 20:78–86

30. Boskey AL, Paschalis EP, McKee M (2002) Mineral and matrix changes in bones of osteopontin-deficient mice. Calcif Tissue Int (in press)

31. Currey JD, Brear K (1990) Hardness, Young's modulus and yield stress in mammalian mineralized tissues. J Mater Sci Mater Med 1:14–20

32. Weiner S, Wagner HD (1998) The material bone: structure-mechanical function relations. Annu Rev Mater Sci 28:271–298

33. Baldock PA, Thomas GP, Sims NA, Henderson KN, Hollis B, Eisman JA, Gardiner EM (2000) Elevated vitamin D receptor in mature osteoblastic cells reduces calcium deficiency-induced bone loss in transgenic mice (abstract). J Bone Miner Res 15(suppl 1): S370